A macro prediction model for butt-welded (U)HSS connections with softened HAZ

Yan, Rui; Xie, Hui; Yang, Fei; Veljkovic, Milan; Zhao, Xiao lin

DOI
10.1016/j.jcsr.2023.108153

Publication date
2023

Document Version
Final published version

Published in
Journal of Constructional Steel Research

Journal of Constructional Steel Research 211 (2023) 108153

Contents lists available at ScienceDirect

Journal of Constructional Steel Research

journal homepage: www.elsevier.com/locate/jcsr

A macro prediction model for butt-welded (U)HSS connections with softened HAZ

Rui Yan [b,c], Hui Xie [a], Fei Yang [a,*], Milan Veljkovic [c], Xiao-lin Zhao [b]

[a] School of Civil Engineering, Chang'an University, Xi'an 710061, China
[b] Department of Civil and Environmental Engineering, The Hong Kong Polytechnic University, Hong Kong, China
[c] Department of Engineering Structures, Delft University of Technology, Delft, the Netherlands

ARTICLE INFO

Keywords:
Heat-affected zone
High-strength steel
Ultra-high-strength steel
Fully-penetrated butt weld
Tensile resistance
Transverse constraint

ABSTRACT

This paper reports an investigation on the tensile resistance of fully-penetrated butt-welded connections of (ultra-)high-strength steels considering the strength softening of the heat-affected zone (HAZ) and the strengthening due to the transverse constraint. Firstly, a parametric study is carried out to analyse the tensile behaviour of fully-penetrated butt-welded S700 connections using validated finite element (FE) models. Based on the FE results, the effect of the investigated parameters on the ultimate resistance of the connections is quantified. Consequently, a Macro prediction model is proposed, neglecting the detail of HAZ inhomogeneous microstructures but considering five design parameters, which are the width and thickness of the specimen, the width of HAZ, the softening ratio, and the matching ratio. Finally, the proposed Macro model is validated against the available experimental data of fully-penetrated butt-welded (ultra-)high-strength steel connections in literature. The results show that the Macro model is proven successful in accurately quantifying the effect of HAZ, concerning the strength softening and the transverse constraint strengthening, on the tensile resistance of fully-penetrated butt-welded (ultra-)high-strength steel connections. It is also found that 157 and 96 out of 185 experiments are predicted within a 5% deviation range using the Macro model and prEN 1993-1-8:2021, respectively, proving that the Macro model is more consistent with the experimental data compared to the prediction of prEN 1993-1-8:2021.

1. Introduction

Welded connection is a common solution to join elements in steel construction. A weld region can be characterized into three major zones, which are the base material (BM), the heat-affected zone (HAZ), and the weld metal (WM). HAZ is an unmelted region due to the heat input during the welding process. The mechanical property of HAZ is sensitive to several parameters, such as the heat input, the cooling time from 800 °C to 500 °C ($t_{8/5}$), and the manufacturing process of BM [1,2]. The strength of HAZ could be comparable to BM, provided that a set of specific welding parameters are used [3–5]. Otherwise, a significant strength degradation might occur in HAZ, which is more severe for steels with a higher strength grade [2,6,7]. Besides, the strength degradation is significant for structural steels after fire [8,9], even though the maximum temperature (up to 1000 °C) might not be as high as that experienced during welding. The reason is that the cooling rate is very low compared to that in a welding process.

Many experimental studies have been carried out to investigate the tensile behaviour of butt-welded high-strength steel (HSS, 460 MPa $\leq f_y \leq$ 700 MPa) and ultra-high-strength steel (UHSS, $f_y >$ 700 MPa) connections [1,3,6,10–24]. HAZ plays a vital role in the welded connection if HAZ has the lowest strength in the entire weld region. Hence, it is important to know the mechanical properties of HAZ to simulate the behaviour or determine the resistance of the welded connection properly. The stress-strain constitutive model of HAZ has been obtained using different methods [1,2,4,6,14,15,17,19,21,23–27], as introduced in [11]. As the mechanical property of HAZ is closely related to the experienced highest temperature and the cooling time during welding, Stroetmann et al. [1] tested HAZ with different combinations of the highest temperature and the cooling time. The temperature-time history on HAZ was reproduced using a thermal simulation machine. Yan et al. [6] calibrated the stress-strain relationship of HAZ based on tensile tests on coupon specimens with a butt weld in the middle. A linear modification factor was proposed to reduce the measured stress to obtain the stress-strain relationship under the uniaxial stress state. Alternatively, the mechanical properties of HAZ can be obtained through the Vickers

* Corresponding author.
E-mail address: f.yang@chd.edu.cn (F. Yang).

https://doi.org/10.1016/j.jcsr.2023.108153
Received 21 April 2023; Received in revised form 2 August 2023; Accepted 4 August 2023
Available online 10 August 2023

hardness test based on the empirical relationship between hardness and strength [2,25–27].

On the other hand, although HAZ may have a lower strength than BM and WM, the final fracture might not appear at HAZ. The reason is that the resistance of the HAZ cross-section is enhanced by a transverse constraint applied by BM and WM [6]. The appearance of the transverse constraint is due to the stronger mechanical properties of adjacent materials. For example, HAZ is weaker than BM, resulting in a higher plastic strain in HAZ than BM in the loading direction. According to the law of volume conservation for plastic deformation, the plastic strain perpendicular to the loading direction is more significant in HAZ than in BM. However, considering the material continuity at the conjunction of two materials, BM and HAZ must have the same perpendicular strain at the interface, which results in the transverse constraint to mediate the perpendicular strain. Hochhauser et al. [13] tested butt-welded coupon specimens with and without milling. The thickness of unmilled specimens was 6 mm (weld reinforcement remained), while the milled specimen had a thickness varying from 6 mm (weld reinforcement removed) to 2 mm. The test results showed that the tensile strength (resistance over the cross-section area) of the specimen decreases with the decrease of the specimen thickness, indicating that the thickness of the specimen influences the level of the transverse constraint. In addition, it was also found that the weld reinforcement would increase the tensile strength. Yan et al. [11] found that the resistance of a butt-welded connection with a 30% strength degradation in HAZ could be equal to that of BM. Therefore, both the HAZ strength degradation and the enhancement owing to the transverse constraint should be evaluated to provide a safe and economical design recommendation for butt-welded connections.

The latest version of prEN 1993-1-8 [28] allows the use of undermatching welds for steel grades equal to or higher than S460. As the resistance of the welded connection decreases with the decrease of WM strength in general [20], the strengths of BM and WM are considered in the current design rule of prEN 1993-1-8 [28]. However, the failure of welded connection is often governed by HAZ [6,11,13,16,18,20–22,24]. Hence, it is unrealistic to accurately predict the tensile resistance of HSS and UHSS connections without considering the strength of HAZ.

In the present study, a finite element (FE) analysis is carried out to investigate the effect of five parameters on the tensile resistance of fully-penetrated butt-welded connections. The investigated parameters include two material strength parameters: the ultimate strength softening ratio of HAZ to BM and the ultimate strength matching ratio of WM to BM, and three geometry parameters: the thickness of the specimen, the width of the specimen, and the width of HAZ. A prediction model is proposed to calculate the tensile resistance of the butt-welded connection considering all five parameters. The prediction model is suitable for the case where HAZ is the weakest zone in the entire weld region. Finally, the proposed model is validated against the available experimental results in literature. It is worth mentioning that the used HAZ strength and width are not measured from the real construction site. The intention is to use the HAZ strength and width predicted based on the type of base material and welding parameters. However, the relationship between the HAZ material properties and the weld details has not been quantified yet. Further studies are required to establish a reliable model for predicting the HAZ strength and width.

2. Parametric study of butt-welded connections

2.1. Finite element (FE) model

Figure 1 a) presents a weld region of a single V-groove butt weld with the bevel angle, the root face, and the root gap indicated. Normally, a butt weld contains reinforcement on the top and bottom sides of the weld (marked in light blue), which may increase the resistance compared to the connection without reinforcement [13]. As a conservative prediction, the weld reinforcement and the root face are not included in the FE model, as shown in Fig. 1 b). The bevel angle and the root gap of the FE model are 45° and 1 mm, respectively, which are the same as the dimensions used in the experiments conducted by Yan et al. [6,11].

The FE analysis, using the ABAQUS:2021 software package [29], is carried out to investigate the effect of five parameters on the tensile resistance of butt-welded coupon specimens. An example of the FE model is presented in Fig. 2. A quarter of the welded coupon specimen without the grip part is created to reduce the number of elements and increase the computation efficiency. The symmetry boundary condition is applied on Surface B and Surface C, indicating parallel edges within the deformation measuring range. A reference point (RP1) is created at the centre of the entire end surface (Surface A). The reference point controls all translations and rotations of Surface A through a multi-point beam constraint (MPC beam) which establishes a linear relationship between degrees of freedom in RP1 and all nodes on Surface A. The load is applied at RP1 by a displacement in the Y direction. The detailed boundary conditions on Surface B, Surface C, and RP1 are illustrated in Fig. 2. The original coupon specimen FE model was employed to calibrate a material damage model to simulate welded hollow section X-joint. Considering the dimension of the X-joint, an appropriate mesh size is required to avoid excessive elements. It was found that a 0.5 mm mesh size can predict the experimental results accurately with an affordable computational cost [6]. Hence, in the current model, the mesh size within the 50 mm gauge length is equal to or slightly smaller than 0.5 mm, while the remaining part uses a coarse mesh in the loading direction. Note that the length of the gauge part shown in Fig. 2 is 25 mm due to the symmetry feature. The C3D8R element is used throughout the whole model. The quasi-static analysis is performed using an explicit solver with a 100 s period and a 0.001 s target time increment. The employed FE model has been successfully validated against milled coupon specimens [6] and verified against unmilled coupon specimens [11]. Fig. 3 a) shows six welded coupon specimens where three of them were milled to a central layer of 3 mm before testing, and three of them were tested as it is. The corresponding FE models are shown in Fig. 3 b). Based on the methods proposed in [6,10], the dimension and the constitutive model of HAZ are determined. The FE model is validated against the milled coupon specimen and further verified against the unmilled welded coupon specimen, as shown in Fig. 3 c) and d), respectively. Detailed information regarding the validation and verification of FE models is available in [6,11].

2.2. Investigated parameters

In the parametric study, three geometry and two strength parameters

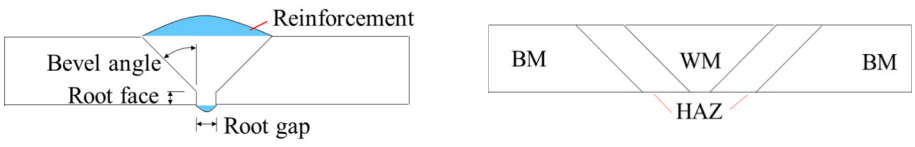

a) Normal weld region. b) Investigated weld region.

Fig. 1. Weld details.

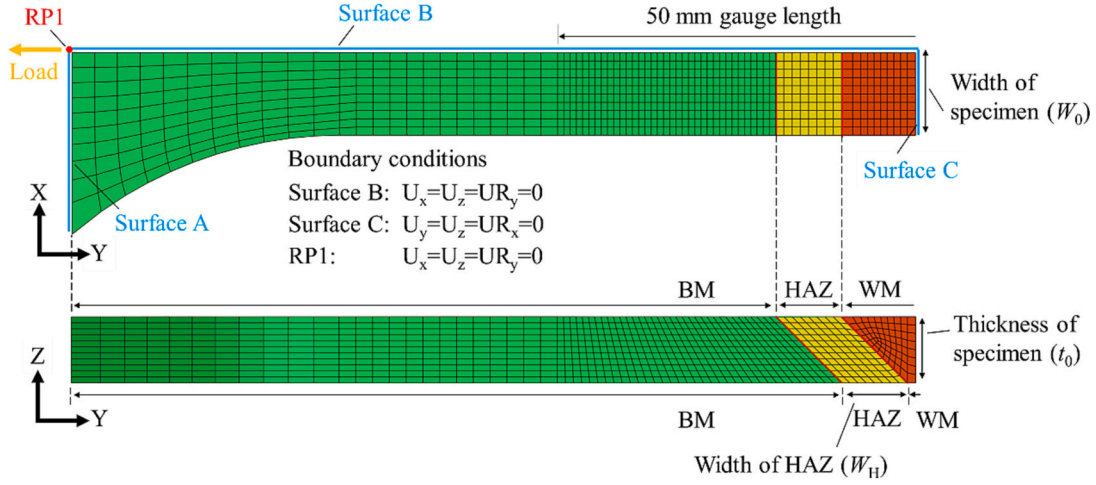

Fig. 2. An example of the finite element (FE) model.

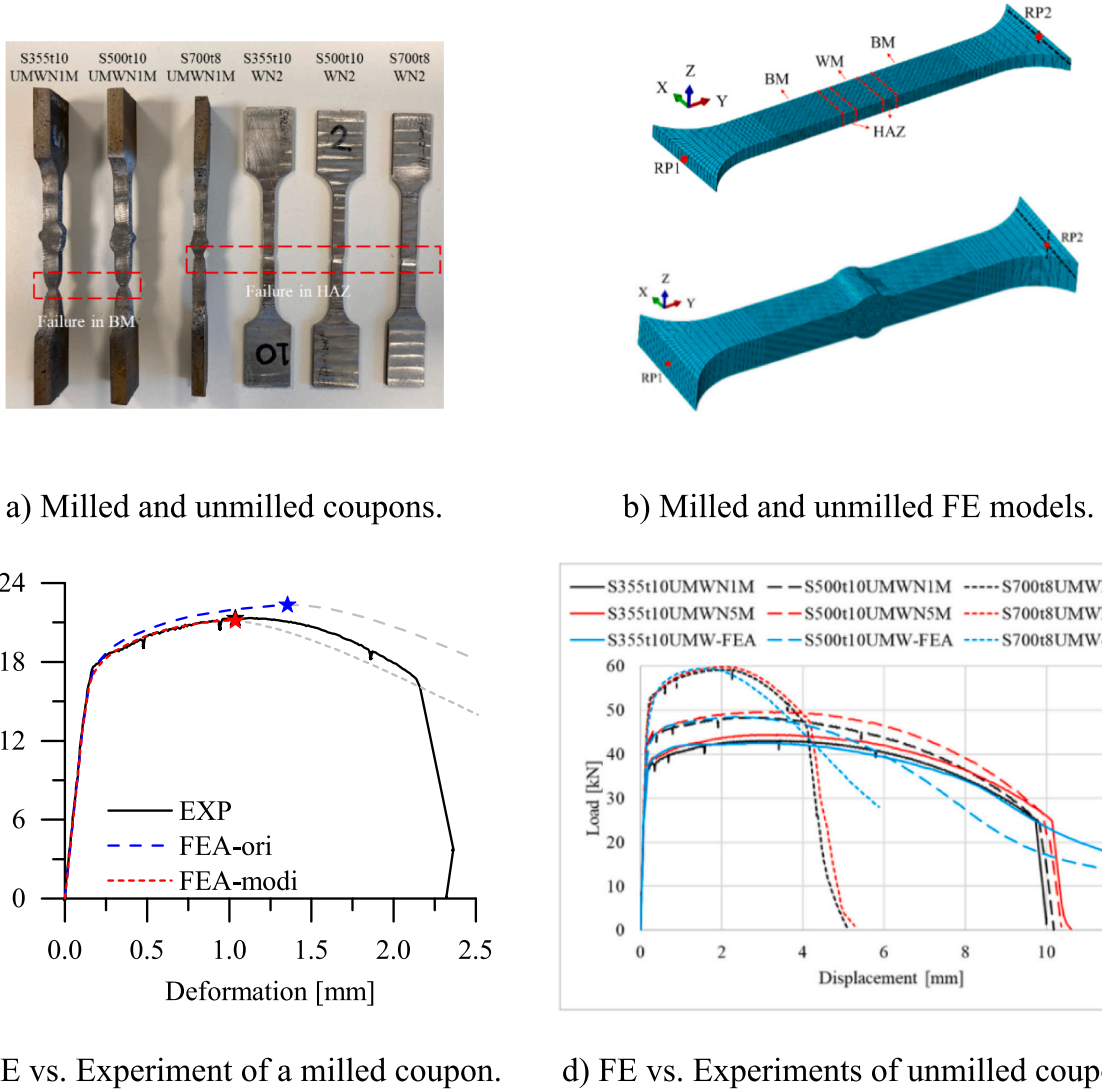

a) Milled and unmilled coupons.

b) Milled and unmilled FE models.

c) FE vs. Experiment of a milled coupon.

d) FE vs. Experiments of unmilled coupons.

Fig. 3. Validation and verification of FE models.

are investigated. The three geometry parameters are the width of specimen W_0, the thickness of specimen t_0, and the width of HAZ W_H, as shown in Fig. 2. Yan et al. [11] found that the majority (92%) of W_H was between 2 mm and 4 mm based on 132 measured W_H from 66 indentation lines on 18 welded samples. Hence, three W_H (2 mm, 3 mm, and 4 mm) are examined. The cross-section dimension may also influence the

level of the transverse constraint applied by BM and WM on HAZ. Three thicknesses and three widths of the specimen are included in the parametric study. The two strength parameters are the softening ratio S_u^{HAZ} and the matching ratio S_u^{WM}, which are the ultimate strengths of the heat-affected zone and the weld metal over that of the base material, respectively. The details of the investigated parameters are summarized in Table 1. Note that the present study focuses on welded connections where HAZ is the weakest part in the weld region. Hence, two strength parameter combinations S_u^{HAZ}=0.8, S_u^{WM}=0.8 and S_u^{HAZ}=0.9, S_u^{WM}=0.8 are excluded from the parametric study. Considering all parameter combinations, 189 models are analysed.

The nominal mechanical property of S700 material is used for BM. According to the latest version of prEN 1993-1-1 [30], the nominal yield strength f_y, ultimate strength f_u, and elongation at fracture ε_f are 700 MPa, 750 MPa, and 0.12, respectively. In addition, the ultimate strain ε_u of S700 material, reported by Yan et al. [11], was approximately 0.03, which is adopted in this study. A 210 GPa Young's modulus E is assumed for all materials.

Yan et al. [11] proposed a semi-empirical constitutive model to determine the mechanical properties of HAZ based on BM, as shown in Eqs. (1)–(3). The yield strength, ultimate strength, and ultimate strain of HAZ are calculated by reducing the yield strength, ultimate strength, and elongation at fracture of BM through reduction factors RF_1, RF_2, and RF_3 in Eqs. (1), (2), and (3), respectively. An RF_3 = 0.8 proposed for S700 welded connections [11] is adopted in this study. Although the strength parameters S_u^{HAZ} and S_u^{WM}concern the ultimate strength, the same reduction factor is also applied to the yield strength, indicating that both RF_1 and RF_2 for HAZ are equal to S_u^{HAZ}. For WM, the yield and ultimate strengths are reduced by S_u^{WM}, while the yield and ultimate strains are kept the same as those of BM. The mechanical properties are presented in Table 2. The yield strain is calculated by f_y/E. The level of the strength reduction is presented at the subscript. For example, $HAZ_{0.7}$ represents HAZ with S_u^{HAZ} equal to 0.7.

$$f_{y,HAZ} = RF_1 \times f_{y,BM} \tag{1}$$

$$f_{u,HAZ} = RF_2 \times f_{u,BM} \tag{2}$$

$$\varepsilon_{u,HAZ} = RF_3 \times \varepsilon_{f,BM} \tag{3}$$

2.3. True stress-strain relationship

The true stress-strain relationship is required in FE analysis. The Swift model [31], as shown in Eq. (4), is employed to generate the true stress-strain relationship of the materials based on the engineering mechanical properties presented in Table 2. $\sigma_{t,S}$ is the true stress predicted by the Swift model. First, the engineering stress and strain are converted to the true stress and strain through Eqs. (5) and (6), respectively. Then, the true stress and true strain at the yield and ultimate points are used to calculate three Swift parameters A, ε_0, and n based on the three conditions presented in Eqs. (7)–(9). Eqs. (7) and (8) are made by substituting the true stress and true strain at the yield point ($\sigma_{t,y}$ and $\varepsilon_{t,y}$) and the ultimate point ($\sigma_{t,u}$ and $\varepsilon_{t,u}$) into Eq. (4), respectively. The last condition Eq. (9) is according to the Considere criterion [32] which is the first derivative of true stress to true strain equal to the true stress at the ultimate point.

Table 1
Details of tested parameters.

Parameters	Values		
t_0 [mm]	4	8	12
W_0 [mm]	10	100	200
W_H [mm]	2	3	4
S_u^{HAZ}[−]	0.7	0.8	0.9
S_u^{WM}[−]	0.8	1.0	1.2

$$\sigma_{t,S} = A(\varepsilon_t + \varepsilon_0)^n \tag{4}$$

$$\sigma_t = \sigma_e(1+\varepsilon_e) \tag{5}$$

$$\varepsilon_t = ln(1+\varepsilon_e) \tag{6}$$

$$\sigma_{t,y} = A(\varepsilon_{t,y} + \varepsilon_0)^n \tag{7}$$

$$\sigma_{t,u} = A(\varepsilon_{t,u} + \varepsilon_0)^n \tag{8}$$

$$\left.\frac{d\sigma_{t,S}}{d\varepsilon_{t,S}}\right|_{\varepsilon_{t,S}=\varepsilon_{t,u}} = \sigma_{t,S}\big|_{\varepsilon_{t,S}=\varepsilon_{t,u}} \tag{9}$$

where ‘t’ and ‘e’ in the subscript stand for true and engineering, respectively.

Yan et al. [33] found that the true stress-strain relationship of HAZ after necking (ultimate strength point) should be generated by the Voce model [34], as shown in Eq. (10), where $\sigma_{t,V}$ is the true stress predicted by the Voce model. Hence, the calculated Swift parameters are used to determine Voce parameters k_0, Q, and β_0 following three continuity conditions at the necking point, which are the true stress (Eq. (11)), the first derivative of true stress (Eq. (12)), and the second derivative of true stress (Eq. (13)) obtained from the Swift model equalling to those from the Voce model. All determined parameters are presented in Table 3. Fig. 4 depicts the generated true stress-true plastic strain relationship for each material.

$$\sigma_{t,V} = k_0 + Q(1 - e^{-\beta_0\varepsilon_t}) \tag{10}$$

$$\sigma_{u,S} = \sigma_{u,V} \tag{11}$$

$$\left.\frac{d\sigma_{t,S}}{d\varepsilon_{t,S}}\right|_{\varepsilon_{t,S}=\varepsilon_{t,u}} = \left.\frac{d\sigma_{t,V}}{d\varepsilon_{t,V}}\right|_{\varepsilon_{t,S}=\varepsilon_{t,u}} \tag{12}$$

$$\left.\frac{d^2\sigma_{t,S}}{d\varepsilon_{t,S}^2}\right|_{\varepsilon_{t,S}=\varepsilon_{t,u}} = \left.\frac{d^2\sigma_{t,V}}{d\varepsilon_{t,V}^2}\right|_{\varepsilon_{t,S}=\varepsilon_{t,u}} \tag{13}$$

2.4. FE results

The reaction force and the deformation based on a 50 mm gauge length are extracted from the FE analysis results. Stress is calculated by dividing the reaction force by the cross-section area. As the FE model is a quarter of the complete specimen, the deformation is measured from a point 25 mm from Surface C in Fig. 2. The stress-deformation relationship and the necking location of three FE models with different levels of transverse constraint are presented in Figs. 5 and 6, respectively. The name of FE model consists of the parameters in order of t_0-W_H-W_0-S_u^{WM}-S_u^{HAZ}. For example, 8–3–100-10-07 represents the model with 8 mm thickness, 3 mm HAZ width, 100 mm specimen width, 1.0 matching ratio, and 0.7 softening ratio. The ultimate strength of BM is plotted as a reference. All three FE models have the same level of material softening in HAZ (S_u^{HAZ}= 0.7). With the decrease of W_H and the increase of t_0, W_0, and S_u^{WM}, the ultimate strength of the FE model gradually increases. And the ultimate strength of 12–2–200-12-07 model is almost identical to that of BM, indicating that the transverse constraint may increase the resistance of the HAZ cross-section by 30%. It is worth mentioning that the necking occurs in WM for the FE model 4–4–10-08-07, while the high strain concentrates in HAZ for the FE models 8–3–100-10-07 and 12–2–200-12-07. The reason for the necking in WM is that the BM applies a strong transverse constraint on HAZ, leading to a higher resistance in HAZ than WM. Moreover, the FE model 4–4–10-08-07 has the lowest level of transverse constraint among all models with a 0.8 matching ratio and a 0.7 softening ratio, as the other models have either a greater thickness, a larger width, or a narrower HAZ width compared to the FE model 4–4–10-08-07. With a more significant transverse

Table 2
Engineering mechanical properties of BM, HAZ, and WM.

	BM	$HAZ_{0.7}$	$HAZ_{0.8}$	$HAZ_{0.9}$	$WM_{0.8}$	$WM_{1.0}$	$WM_{1.2}$
f_y [MPa]	700	490	560	630	560	700	840
ε_y [−]	0.0033	0.0023	0.0027	0.0030	0.0027	0.0033	0.0040
f_u [MPa]	750	525	600	675	600	750	900
ε_u [−]	0.03	0.096	0.096	0.096	0.03	0.03	0.03
ε_f [−]	0.12	–	–	–	–	–	–

Table 3
Determined parameters of constitutive models.

		BM	$HAZ_{0.7}$	$HAZ_{0.8}$	$HAZ_{0.9}$	$WM_{0.8}$	$WM_{1.0}$	$WM_{1.2}$
Swift model	A	852	745	851	956	683	852	1020
	ε_0	−0.00257	0.0318	0.0310	0.0302	−0.00176	−0.00257	−0.00327
	n	0.0270	0.123	0.123	0.122	0.0278	0.0270	0.0263
Voce model	k_0	–	501	572	644	–	–	–
	Q	–	155	177	199	–	–	–
	β_0	–	7.10	7.15	7.20	–	–	–

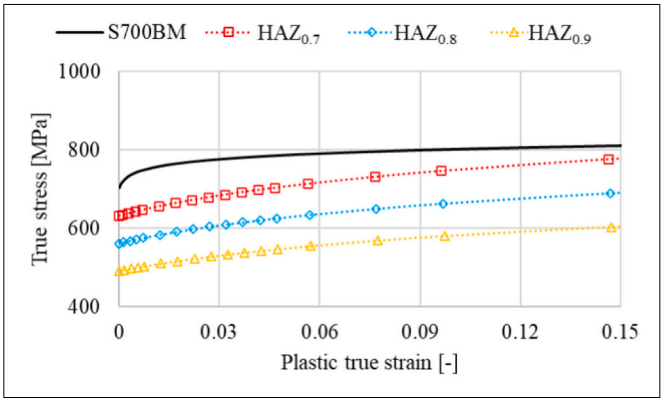

a) HAZ and BM.

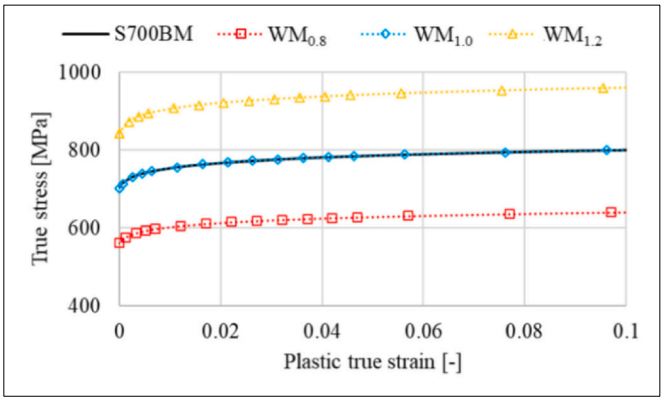

b) WM and BM.

Fig. 4. True stress-true plastic strain relationship.

constraint on HAZ, it is more unlikely to fail in HAZ, indicating that all models with a 0.8 matching ratio and a 0.7 softening ratio would fail in WM. Note that although the material damage model is not employed in this study, the necking position could indicate the position of the final failure.

An ultimate resistance ratio, which is the ultimate resistance of the FE model over BM, is calculated for each model, as shown in Table 4. The model with a resistance ratio equal to or above 0.95 is marked in green. It can be seen that, in the investigated range of parameters, all

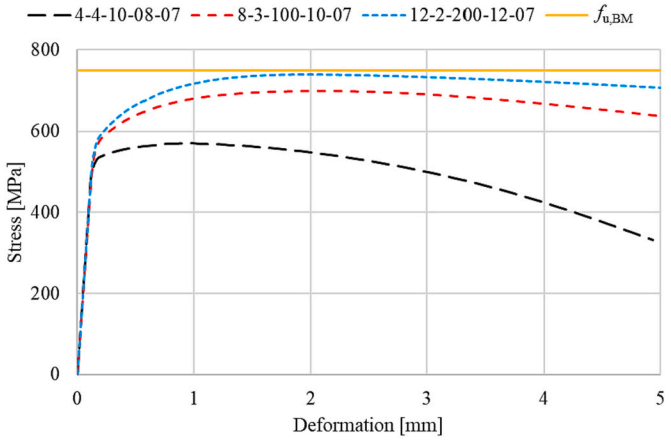

Fig. 5. Stress-deformation relationship.

models with a 0.9 softening ratio have an ultimate resistance maximally 5% lower than that of BM. For models with a 0.8 softening ratio, a 95% BM ultimate resistance can be reached, provided that the width of the specimen is not <100 mm.

3. Prediction model

3.1. Derivation of the proposed macro model

Equation (14) is proposed to predict the ultimate resistance R_u of a butt-welded connection. The ultimate strength of HAZ $f_{u,HAZ}$ can be substituted by the ultimate strength of BM $f_{u,BM}$ times the softening ratio. A constraint factor β_c is proposed to consider the strength enhancement due to the transverse constraint. The level of the transverse constraint depends on five parameters, as investigated in the parametric study. A strength factor β_s and a geometry factor β_g are proposed to consider the strength and geometry effects separately. As the level of the transverse constraint depends on the strength difference between the strong material (WM and BM) and the weak material (HAZ), the strength factor is defined by the product of $f_{u,BM}/f_{u,HAZ}$ and $f_{u,WM}/f_{u,HAZ}$, as shown in Eq. (15). Similarly, the geometry factor is defined by the product of t_0/H_W and W_0/H_W (see Eq. (16)).

$$R_u = f_{u,HAZ} t_0 W_0 \beta_c = f_{u,BM} S_u^{HAZ} t_0 W_0 \beta_c \quad (14)$$

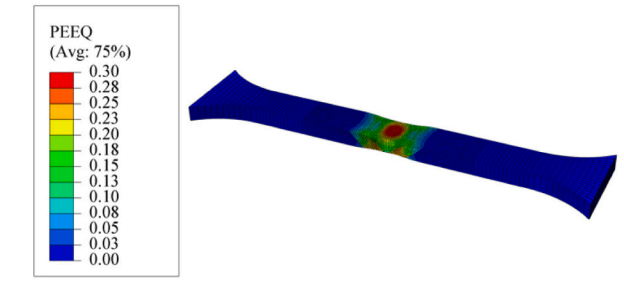

a) 4-4-10-08-07

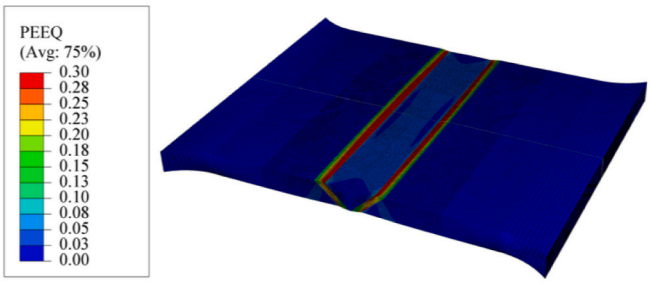

b) 8-3-100-10-07

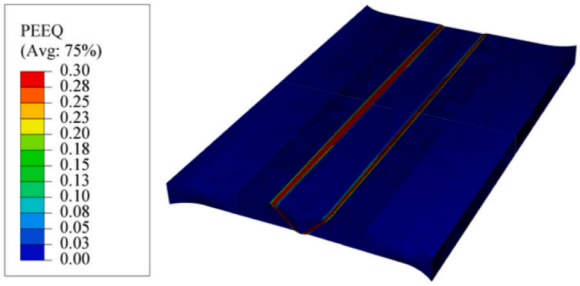

c) 12-2-200-12-07

Fig. 6. Necking location in three FE models.

Table 4
Ultimate resistance ratio.

			W_0	10			100			200		
			t_0	4	8	12	4	8	12	4	8	12
S_u^{HAZ}	S_u^{WM}	H_W										
0.7	0.8	4		0.76	0.78	0.79	0.85	0.86	0.87	0.86	0.88	0.89
		3		0.78	0.79	0.79	0.86	0.88	0.88	0.87	0.89	0.90
		2		0.79	0.80	0.80	0.88	0.89	0.89	0.89	0.90	0.91
	1.0	4		0.82	0.85	0.87	0.88	0.92	0.93	0.89	0.93	0.95
		3		0.84	0.88	0.90	0.90	0.93	0.94	0.91	0.95	0.96
		2		0.88	0.91	0.93	0.93	0.95	0.96	0.94	0.97	0.97
	1.2	4		0.83	0.86	0.88	0.89	0.93	0.95	0.90	0.94	0.96
		3		0.86	0.90	0.91	0.92	0.95	0.97	0.92	0.96	0.98
		2		0.90	0.93	0.95	0.94	0.97	0.98	0.95	0.98	0.99
0.8	1.0	4		0.89	0.92	0.93	0.96	0.97	0.97	0.98	1.00	1.00
		3		0.91	0.94	0.95	0.97	0.98	0.98	0.99	1.01	1.01
		2		0.93	0.96	0.97	0.99	0.99	0.99	1.00	1.01	1.02
	1.2	4		0.91	0.94	0.96	0.98	1.00	1.01	0.99	1.01	1.03
		3		0.94	0.97	0.98	0.99	1.01	1.02	1.00	1.02	1.03
		2		0.97	0.99	1.00	1.00	1.01	1.02	1.02	1.03	1.04
0.9	1.0	4		0.95	0.97	0.97	0.99	0.99	0.99	1.02	1.02	1.02
		3		0.96	0.97	0.98	1.00	1.00	1.00	1.02	1.02	1.02
		2		0.97	0.98	0.99	1.00	1.00	1.00	1.02	1.02	1.03
	1.2	4		0.97	0.99	1.00	1.01	1.02	1.03	1.03	1.04	1.04
		3		0.99	1.00	1.00	1.01	1.02	1.03	1.03	1.04	1.05
		2		1.00	1.00	1.00	1.01	1.02	1.03	1.03	1.04	1.05

$$\beta_s = \frac{f_{u,BM}}{f_{u,HAZ}} \times \frac{f_{u,WM}}{f_{u,HAZ}} = \frac{1}{S_u^{HAZ}} \times \frac{S_u^{WM}}{S_u^{HAZ}} = \frac{S_u^{WM}}{S_u^{HAZ\,2}} \tag{15}$$

$$\beta_g = \frac{t_0}{H_W} \times \frac{W_0}{H_W} = \frac{t_0 W_0}{H_W^2} \tag{16}$$

$$\beta_c = min\left(a_1\beta_s + a_2\beta_g^{a_3}, \frac{1}{S_u^{HAZ}}\right) \tag{17}$$

$$a_1 = 0.138, \quad a_2 = 0.871, \quad a_3 = 0.0363$$

All FE models presented in Table 4 are used to derivate the prediction model. The constraint factor can be calculated for each FE model following Eq. (14). The constraint factor is plotted against the geometry factor in Fig. 7 a). The data points are sorted into four groups by the softening ratio. Although three softening ratios were tested in the parametric study, one extra softening ratio of "0.8*" is identified. The reason is that the FE models with a 0.7 softening ratio and a 0.8 matching ratio fail in WM, indicating that the resistance of these models is governed by the material (WM) which is 20% weaker than the base material. Consequently, the trend of this set of data is closer to the "0.8" series than the "0.7" series. Hence, a "0.8*" category is defined independently to visualise the data properly. Fig. 7 a) shows that the relationship between the constraint factor and the geometry factor follows the power law. Hence, a power law with two parameters (a_2 and a_3) is assumed in Eq. (17). Fig. 7 b) presents five examples of the relationship between the constraint factor and the geometry factor. The data is sorted

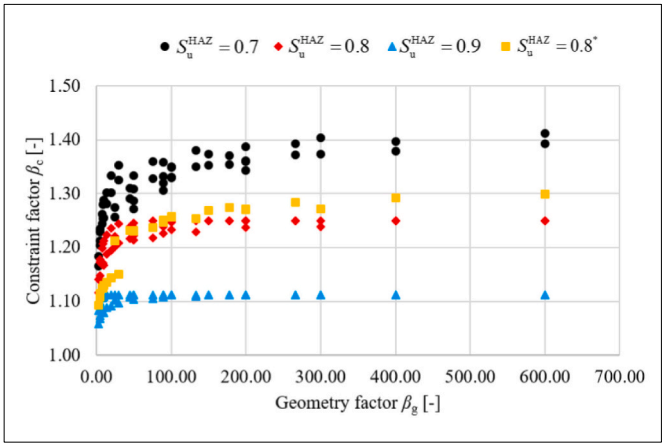

a) Constraint factor vs. Geometry factor.

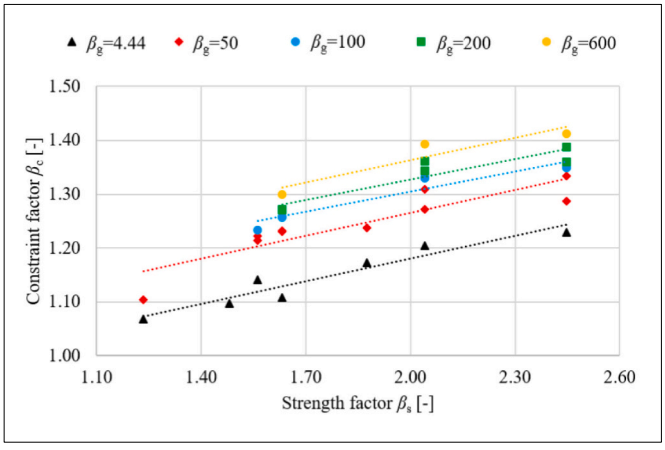

b) Constraint factor vs. Strength factor.

Fig. 7. Effect of geometry and strength factors on the level of transverse constraint.

by the geometry factor. It can be seen that the constraint factor shows a linear correlation to the strength factor, as shown by the dot trend lines, which are generated by fitting the data points. Note that the dot lines are only used for displaying the trend but not deriving the parameters. Hence, one parameter a_1 is assumed for the strength factor in Eq. (17). As the constraint effects resulted from the geometry and the strength difference are not coupled, the constraint factors are simply combined linearly in Eq. (17). Note that the models with strength equal to BM are excluded from Fig. 7 b), as the constraint effect of those models is limited by the strength of BM, and those data points would blur the trend shown in the figure. Since the ultimate resistance of the welded connection is limited by BM, an up limit of $1/S_u^{HAZ}$ is stipulated for the constraint factor, as shown in Eq. (17).

The three parameters (a_1, a_2, and a_3) are fitted by minimising the absolute difference between the FE and predicted constraint factor considering all FE models. The determined parameters are shown in Eq. (17). The proposed equation predicts the ultimate resistance of all 189 FE models with a maximum of 5% deviation, as shown in Fig. 8. The mean and Coefficient Of Variation (COV) are 1.00 and 0.015, respectively.

3.2. Validation of the proposed macro model

The proposed model is further validated against the tensile test results of butt-welded connections in literature. The width of HAZ, the softening ratio, and the matching ratio are calculated based on the hardness result, except for the strength of HAZ in [6,11], which is calibrated against tensile coupon tests. Fig. 9 presents an example of the hardness result used to determine the softening and matching ratios. The softening ratio is determined as the minimum hardness of HAZ over the average hardness of BM (HAZ_{min}/BM_{ave}). The matching ratio is the average hardness of WM over the average hardness of BM (WM_{ave}/BM_{ave}). The width of HAZ is characterized by two boundary points which have the same hardness as BM. The available data in literature is summarized in Appendix.

It is worth mentioning that the softening ratio and the matching ratio in the proposed model are based on the ultimate strength of the material, while the hardness result is used in the calculation. Although the yield strength and the ultimate strength could be estimated by the hardness value [35], it was found that indentation formed in the Vickers hardness test is associated with an approximately 8% strain [36]. In addition, the hardness of HAZ is measured from a single point, while an equivalent strength representing the entire HAZ should be used. Hence, the calculated softening ratio and hardening ratio might deviate from the actual values. The ultimate strength of HAZ was calibrated in [6,11], and the ultimate resistance of all 40 specimens is predicted with a maximum of 5% deviation, except for one specimen with a 6% overestimation. Fig. 10 compares the Macro model results to all available experimental results in literature. It can be seen that all resistances are well predicted with <10% deviation, except for two specimens with a 14% resistance underestimation. The mean and COV are 1.01 and 0.040, respectively.

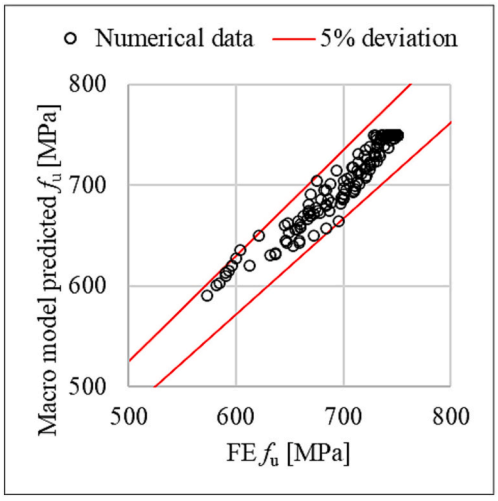

Fig. 8. Macro model prediction vs. FE results.

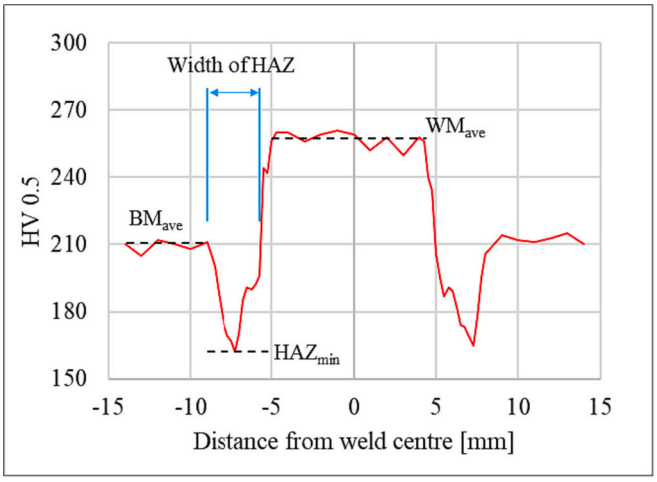

Fig. 9. Evaluation of the hardness result.

Although a 45° bevel angle is used in FE models, the Macro model predicts the experimental results (with the bevel angle varying between 22.5° and 45°, and 0° for a laser weld) well without distinct over- or underestimation. It indicates that the bevel angle might not be influential for the ultimate resistance of a butt weld. A possible explanation for this phenomenon is that the dimension of the width is larger than the thickness. Consequently, the transverse constraint is mainly in the width direction, and the interaction between different layers is insignificant.

The suggested value of 0.8 for RF_3 [11] is adopted in this study. A question is raised on the applicability of the Macro model on butt welds where $RF_3 = 0.8$ is not valid. The adopted value of RF_3 is a conservative estimation. The lower HAZ ultimate strain $\varepsilon_{u,HAZ}$ would result in a lower level of the transverse constraint, consequently, a conservative prediction on the ultimate resistance of the butt weld. Besides, the experimental varying range of the $\varepsilon_{u,HAZ}/\varepsilon_{f,BM}$ ratio for S700 materials was mainly 0.8–0.92 [11]. With a 0.12 difference in terms of the $\varepsilon_{u,HAZ}/\varepsilon_{f,BM}$ ratio, $\varepsilon_{u,HAZ}$ only differs by 0.0144, which is expected to have a limited influence on the ultimate resistance. The comparison between the Macro model prediction and the experiments, as shown in Fig. 10, also proves that the $RF_3 = 0.8$ does not decisive, as $RF_3 = 0.8$ is not valid for all experiments.

3.3. Comparison of the proposed macro model and the model in prEN 1993-1-8

The latest version of prEN 1993-1-8 [28] stipulates that the strength of butt-welded connections in steel grades equal to or higher than S460 may be determined by Eq. (18).

$$\sigma_{v,Rd} = \frac{0.85 \times (0.9 f_{u,BM}) + 0.15 f_{u,WM}}{\gamma_{M2}} \tag{18}$$

where $f_{u,BM}$ and $f_{u,WM}$ are the ultimate strength of BM and WM. γ_{M2} is the partial factor for resistance of cross-sections in tension to fracture. The partial factor is not included in the following calculation in order to obtain the ultimate resistance of the connection instead of a design resistance. Note that $f_{u,WM}$ should be calculated by the strength of WM times the matching ratio $f_{u,BM} \times S_u^{WM}$.

The prediction of prEN 1993-1-8 (EC3) is compared to the FE results and the experiments in Figs. 11 and 12, respectively. The ultimate

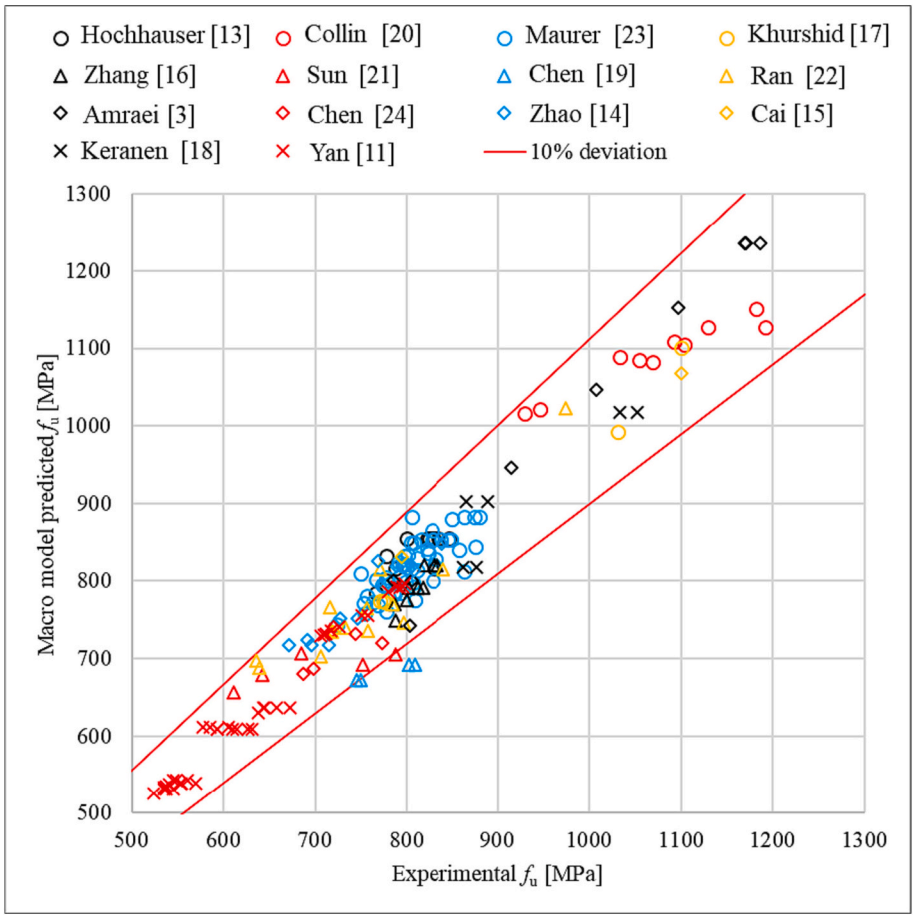

Fig. 10. Validation of the prediction model.

resistance of 94 out of 189 FE models is predicted with a maximum of 5% deviation. The number of models increases to 179 if the maximum deviation is 10%. The mean and COV of EC3 predicted FE results are 0.98 and 0.056, respectively. 96 out of 185 and 163 out of 185 experiments are predicted with a maximum of 5% and 10% deviation using the EC3 model, respectively. The mean and COV of EC3 predicted FE results are 0.99 and 0.073, respectively. In general, the EC3 model tends to overestimate the ultimate resistance if a significant strength degradation occurs in HAZ.

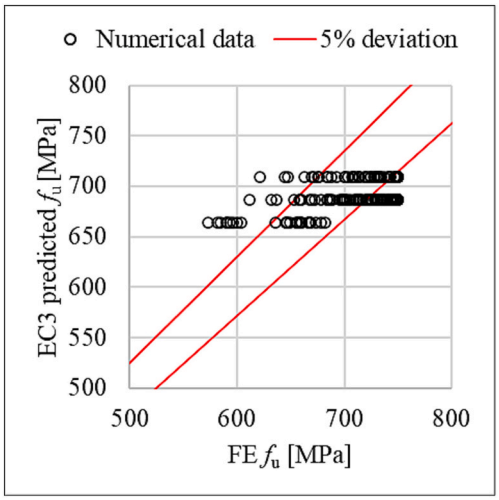

Fig. 11. EC3 prediction vs. FE results.

Table 5 summarises the statistical coefficients of the Macro model and EC3 predictions. Comparing the results of the EC3 model (Section 3.3) to the Macro model (Section 3.1 and Section 3.2), it is evident that the Macro model shows a better prediction on the ultimate resistance of fully-penetrated butt-welded connections.

4. Conclusions

The present study focuses on the tensile resistance of fully-penetrated butt-welded high-strength steel and ultra-high-strength steel connections with a softened heat-affected zone (HAZ). The Macro model is proposed based on the finite element (FE) analysis results (maximum 200 mm wide) and validated against available experiments in literature (maximum 100 mm wide). The following conclusions are drawn:

1. The base material and the weld metal apply a transverse constraint on HAZ. The FE result shows that, within the range of the investigated parameters, the transverse constraint may increase the tensile resistance of the HAZ cross-section by at least 5%. A maximum of approximately 30% resistance enhancement is observed in the FE results.
2. Two factors are proposed to represent five parameters. The strength factor β_s, considering the softening ratio and the matching ratio, shows a linear relationship to the constraint factor β_c. The effect of the geometry factor β_g, considering the width of the specimen, the thickness of the specimen, and the width of HAZ, on the constraint factor β_c can be described by the power law.
3. The proposed Macro model shows better agreement for the ultimate resistance of the fully-penetrated butt-welded connection compared to the model in prEN 1993-1-8 [28] (EC3 model). The Macro model

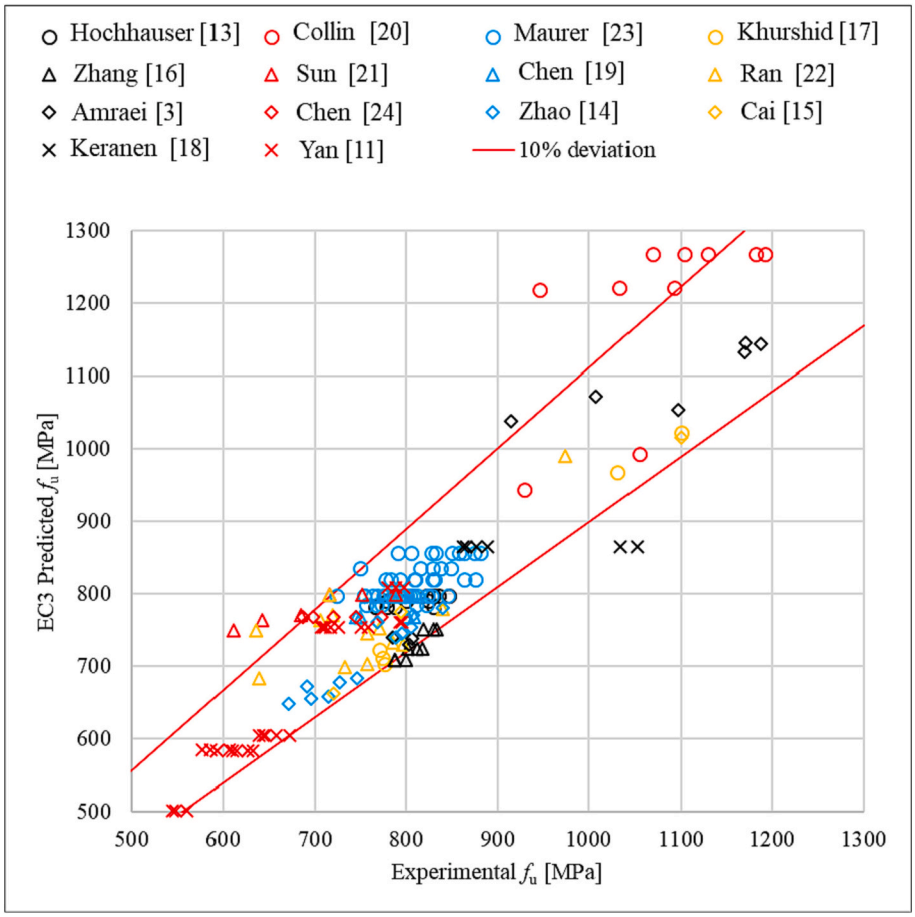

Fig. 12. EC3 prediction vs. experiments in literature.

Table 5
Statistical coefficients.

	Macro model		EC3	
	Mean	COV	Mean	COV
FE results	1.00	0.015	0.98	0.056
Experiments	1.01	0.040	0.99	0.073

predicts the ultimate resistance of all 189 FE models with a maximum of 5% deviation, while only 94 models are within this deviation range using the EC3 model. The coefficient of variation (COV) of the Macro and EC3 models are 0.015 and 0.056, respectively. Regarding the experiments in literature, the Macro model and the EC3 model have 183 and 163 out of 185 experiments predicted with a maximum of 10% deviation, respectively. 157 and 96 experiments are within a 5% deviation range using the Macro model and the EC3 model, respectively. The COV of the Macro and EC3 models are 0.040 and 0.073, respectively.

4. The softening ratio is calculated based on the hardness result in literature. For future studies, a hardness testing force, such as HV 0.5 or HV 5, should be proposed to represent the equivalent strength of HAZ.

Limits of the Macro model are related to the dimension of the specimens available in literature and prediction of HAZ material properties. For future work, the following two research lines are interesting to investigate further: (1) Consider wider specimens in FE analysis and in experiments; (2) Establish a reliable model which can predict the width and strength of HAZ based on the type of base material and the welding parameters.

CRediT authorship contribution statement

Rui Yan: Conceptualization, Methodology, Validation, Formal analysis, Investigation, Data curation, Writing – original draft, Writing – review & editing, Visualization. **Hui Xie:** Software, Validation, Formal analysis, Data curation. **Fei Yang:** Methodology, Investigation, Writing – review & editing, Visualization. **Milan Veljkovic:** Supervision, Writing – review & editing. **Xiao-lin Zhao:** Supervision, Writing – review & editing.

Declaration of Competing Interest

The authors declare that they have no known competing financial interests or personal relationships that could have appeared to influence the work reported in this paper.

Data availability

The raw/processed data can be shared on request.

Acknowledgements

None.

Appendix A. Appendix

Experimental data of butt-welded coupon specimens.

Specimen	Exp [MPa]	Pre [MPa]	Pre/Exp [-]	$f_{u,BM}$ [MPa]	t_0 [mm]	W_0 [mm]	W_H [mm]	S_u^{WM} [-]	S_u^{HAZ} [-]	BA [°]
Yan et al. [11].										
S700t10WN2	780	786	1.01	904	3.0	7.9	3.50	0.86	0.81	45
S700t10WN3	789	792	1.00	904	3.0	8.0	3.50	0.86	0.82	45
S700t10WN4	798	797	1.00	904	2.9	7.6	3.50	0.86	0.83	45
S700t8WN2	712	733	1.03	833	3.0	10.0	3.00	0.94	0.79	45
S700t8WN3	717	736	1.03	833	3.0	10.0	3.00	0.94	0.79	45
S700t8WN3M	726	742	1.02	833	3.0	10.1	3.00	0.94	0.80	45
S700t8WN4	709	731	1.03	833	2.9	9.9	3.00	0.94	0.78	45
S700t8WN4M	707	729	1.03	833	3.0	10.0	3.00	0.94	0.78	45
S700t5WN3	795	793	1.00	841	2.9	19.9	3.00	0.93	0.85	45
S700t5WN4	793	791	1.00	841	3.0	19.9	3.00	0.93	0.85	45
S500t10WN2	632	608	0.96	608	3.0	7.9	4.00	1.28	1.04	45
S500t10WN3	593	608	1.03	608	3.0	8.0	4.00	1.28	0.97	45
S500t10WN3M	593	608	1.03	608	3.0	8.0	4.00	1.28	0.97	45
S500t10WN4	615	608	0.99	608	3.0	8.1	4.00	1.28	1.01	45
S500t10WN4M	610	608	1.00	608	3.0	8.0	4.00	1.28	1.00	45
S500t8WN2	606	612	1.01	612	3.0	10.0	4.00	1.27	0.96	45
S500t8WN3	577	612	1.06	612	3.0	9.9	4.00	1.27	0.92	45
S500t8WN4	586	612	1.04	612	3.0	9.9	4.00	1.27	0.94	45
S500t4WN2	643	637	0.99	637	3.0	19.8	5.00	1.23	0.94	45
S500t4WN3	645	637	0.99	637	3.0	9.9	5.00	1.23	0.94	45
S500t4WN4	638	631	0.99	637	3.0	9.9	5.00	1.23	0.92	45
S355t10WN2	569	539	0.95	539	3.0	8.0	4.00	1.06	1.00	45
S355t10WN3	537	535	1.00	539	3.0	8.1	4.00	1.06	0.95	45
S355t10WN3M	524	526	1.00	539	3.0	8.0	4.00	1.06	0.92	45
S355t10WN4	541	537	0.99	539	3.0	8.0	4.00	1.06	0.95	45
S355t10WN4M	535	533	1.00	539	3.0	8.0	4.00	1.06	0.94	45
S355t8WN2	545	531	0.97	531	3.0	10.1	3.50	1.08	0.98	45
S355t8WN3	535	531	0.99	531	3.0	9.9	3.50	1.08	0.97	45
S355t8WN4	538	531	0.99	531	3.0	10.0	3.50	1.08	0.97	45
S355t5WN2	561	543	0.97	543	3.0	16.0	4.00	1.06	0.98	45
S355t5WN3	549	543	0.99	543	3.0	15.6	4.00	1.06	0.96	45
S355t5WN4	545	543	1.00	543	3.0	16.0	4.00	1.06	0.95	45
S700t8UMWN1M	758	755	1.00	833	7.9	9.9	3.00	0.94	0.79	45
S700t8UMWN5M	751	756	1.01	833	7.9	10.1	3.00	0.94	0.79	45
S500t10UMWN1M	627	608	0.97	608	9.9	7.8	3.20	1.28	1.00	45
S500t10UMWN5M	626	608	0.97	608	9.9	8.0	3.20	1.28	1.00	45
S355t10UMWN1M	553	539	0.98	539	9.9	7.9	3.30	1.06	0.95	45
S355t10UMWN5M	555	539	0.97	539	9.9	8.1	3.30	1.06	0.95	45
S500t4UMWN3	673	637	0.95	637	3.9	59.8	3.50	1.23	0.93	45
S500t4UMWN4	658	637	0.97	637	4.0	59.7	3.50	1.23	0.93	45
Hochhauser et al. [13].										
With reinforcement	847	855	1.01	855	6	20	1.97	1.12	0.88	25
	830	817	0.98	855	6	20	3.59	1.00	0.84	25
Without reinforcement	835	855	1.02	855	6	20	1.99	1.12	0.88	25
	824	855	1.04	855	6	20	2.45	1.06	0.87	25
	788	817	1.04	855	6	20	3.59	1.00	0.84	25
	829	855	1.03	855	5	20	2.16	1.12	0.88	25
	830	855	1.03	855	4	20	2.21	1.12	0.88	25
	800	855	1.07	855	4	20	1.96	1.06	0.87	25
	778	801	1.03	855	4	20	4.10	1.00	0.84	25
	822	855	1.04	855	3	20	2.20	1.12	0.88	25
	778	833	1.07	855	2	20	2.51	1.06	0.87	25
	766	785	1.03	855	2	20	4.00	1.00	0.84	25
Zhao [14].										

.

S550QT-1.0	746	752	1.01	752	20	25	2.15	0.96	0.90	30
S550TMCP-1.0	715	717	1.00	717	20	25	1.89	1.02	0.90	30
S550QT-1.5	727	752	1.03	752	20	25	2.15	0.91	0.89	30
S550TMCP-1.5	672	717	1.07	717	20	25	2.81	0.93	0.89	30
S550QT-1.9	692	724	1.05	752	20	25	3.85	0.85	0.83	30
S550TMCP-1.9	696	717	1.03	717	20	25	4.36	0.99	0.87	30
S690QT-1.0	806	819	1.02	819	20	25	1.64	1.04	0.89	30
S690TMCP-1.0	839	848	1.01	848	20	25	3.89	1.03	0.85	30
S690QT-1.5	796	818	1.03	819	20	25	2.76	0.97	0.83	30
S690TMCP-1.5	769	826	1.07	848	20	25	1.92	0.88	0.79	30
S690QT-1.9	789	819	1.04	819	20	25	3.16	0.93	0.86	30
S690TMCP-1.9	808	813	1.01	848	20	25	3.00	0.95	0.79	30
Cai et al. [15].										
QT550-1.5-F7	720	734	1.02	734	20	10	2.15	0.91	0.89	30
QT690-1.5-F7	794	831	1.05	852	20	10	2.76	0.97	0.83	30
QT890-1.5-F7	1100	1068	0.97	1121	20	10	3.38	0.94	0.82	30
Zhang and Kannengiesser [16].										
A1	818	792	0.97	792	6	25	0.78	1	0.91	30
A2	802	792	0.99	792	6	25	0.64	1	0.92	30
A3	812	792	0.98	792	6	25	0.36	1	0.91	30
B1	787	770	0.98	775	6.5	25	1	1	0.78	30
B2	788	750	0.95	775	6.5	25	0.9	1	0.74	30
B3	800	775	0.97	775	6.5	25	0.63	1	0.83	30
C1	819	821	1.00	821	8	25	1.07	1	0.87	30
C2	830	821	0.99	821	8	25	0.97	1	0.87	30
C3	833	821	0.99	821	8	25	0.70	1	0.91	30
Amraei et al. [3].										
S700-LW	806	801	0.99	801	8	80	1.30	1.04	0.96	30
S700-LQ	785	801	1.02	801	8	80	3.39	1.05	0.84	30
S700-HQ	803	742	0.92	801	8	80	5.16	0.97	0.77	30
S960-LW	1097	1152	1.05	1152	8	80	1.37	1.00	0.77	30
S960-LQ	1008	1047	1.04	1152	8	80	5.62	1.11	0.72	30
S960-HQ	915	946	1.03	1152	8	80	7.32	0.91	0.66	30
S1100-LW	1171	1235	1.05	1235	8	80	0.91	1.08	0.97	30
S1100-LQ	1187	1235	1.04	1235	8	80	2.12	1.07	0.97	30
S1100-HQ	1170	1235	1.06	1235	8	80	2.60	1.01	0.90	30
Khurshid et al. [17].										
S700-2	777	773	1.00	774	6	30	2.09	0.95	0.85	45
S700-6	774	774	1.00	774	6	30	2.09	1.03	0.86	45
S700-10	771	774	1.00	774	6	30	2.13	1.13	0.84	45
S960-4	1031	993	0.96	1101	6	30	1.25	0.76	0.73	45
S960-8	1101	1101	1.00	1101	6	30	1.25	1.10	0.86	45
Keranen et al. [18]. Note: The 0 degree bevel angle is for the laser weld.										
HMAG-0°C	877	818	0.93	1131	2	12	2.23	0.88	0.55	25
LMAG-0°C	889	903	1.02	1131	2	12	3.47	0.88	0.70	25
Laser-0°C	1052	1018	0.97	1131	2	12	1.16	1.01	0.74	0
HMAG-20°C	862	818	0.95	1131	2	12	2.23	0.88	0.55	25
LMAG-20°C	866	903	1.04	1131	2	12	3.47	0.88	0.70	25
Laser-20°C	1034	1018	0.98	1131	2	12	1.16	1.01	0.74	0
Chen et al. [19].										
BJ-3.2-1	809	693	0.86	838	8	12.5	4.50	1.01	0.67	30
BJ-3.2-2	802	693	0.86	838	8	12.5	4.50	1.01	0.67	30
BJ-5.0-1	750	672	0.90	838	8	12.5	5.50	1.01	0.64	30
BJ-5.0-2	745	672	0.90	838	8	12.5	5.50	1.01	0.64	30
Collin et al. [20]. Note: W1 and W2 denotes two steel grades S960 and S1100, respectively. F1 and F2 are two filler materials PZ6145 and PZ6149, respectively. The strength of each row is the average of three repeated tests.										

W1-F2	1054	1084	1.03	1099	6	24	2.69	0.92	0.87	25
W2-F1	946	1022	1.08	1458	5.5	24	4.79	0.47	0.65	25
W1-F1	929	1017	1.09	1099	6	24	3.35	0.63	0.86	25
W2-F2	1104	1105	1.00	1458	5.5	12	3.73	0.70	0.67	25
	1130	1127	1.00	1458	5.5	24	3.73	0.70	0.67	25
	1182	1151	0.97	1458	5.5	48	3.73	0.70	0.67	25
	1069	1082	1.01	1458	5.5	6	3.73	0.70	0.67	25
	1192	1128	0.95	1458	5.5	96	5.24	0.70	0.64	25
	1093	1108	1.01	1397	12	24	4.56	0.73	0.67	25
	1033	1089	1.05	1397	12	24	4.50	0.73	0.65	40
Sun et al. [21].										
UM1	611	656	1.07	856	10	25	8.72	0.73	0.68	30
UM2	642	678	1.06	856	10	25	8.48	0.85	0.68	30
UM3	685	706	1.03	856	10	25	6.71	0.90	0.70	30
OM-A	716	737	1.03	856	10	25	6.53	1.12	0.68	30
OM-B	751	692	0.92	856	10	25	7.80	1.12	0.60	30
OM-C	788	705	0.89	856	10	25	7.55	1.12	0.63	30
Ran et al. [22]. Note: The symbol "*" represents a double-V groove weld with 22.5° on one side and 30° on the other side.										
B11	639	689	1.08	771	10	25	2.50	0.81	0.75	30
B12	733	740	1.01	771	10	25	2.06	0.94	0.79	30
B14	785	771	0.98	771	10	25	1.61	1.24	0.81	30
C13	758	736	0.97	767	10	25	3.42	1.00	0.81	30
C14	796	747	0.94	767	10	25	3.91	1.25	0.78	30
C22	757	765	1.01	832	20	25	3.24	0.87	0.76	*
C23	771	815	1.06	832	20	25	1.96	0.93	0.79	*
C24	840	816	0.97	832	20	25	2.76	1.15	0.76	*
D14	974	1023	1.05	1108	10	25	3.15	0.86	0.79	30
SC11L	636	697	1.10	856	10	100	6.61	0.73	0.68	30
SC12L	706	703	1.00	856	10	100	9.26	0.85	0.68	30
SC13L	719	734	1.02	856	10	100	5.92	0.90	0.69	30
SC14L	716	767	1.07	856	10	100	6.12	1.12	0.68	30
Maurer [23]. Note: Four specimens in the group "Matching type investigation" is repeatedly used in the group "Heat input investigation", as marked in green.										
Matching type investigation	846	854	1.01	854	5	30	2.33	1.12	0.86	25
	823	836	1.02	854	5	30	3.46	1.12	0.83	25
	796	820	1.03	854	5	30	4.15	1.12	0.82	25
	792	805	1.02	854	5	30	4.45	1.12	0.80	25
	776	793	1.02	854	5	30	4.74	1.12	0.78	25
	754	772	1.02	854	5	30	6.04	1.12	0.77	25
	724	744	1.03	854	5	30	8.21	1.12	0.74	25
	822	842	1.02	854	5	30	3.04	1.03	0.85	25
	811	830	1.02	854	5	30	3.54	1.03	0.84	25
	767	802	1.05	854	5	30	4.23	1.03	0.81	25
	773	795	1.03	854	5	30	4.07	1.03	0.80	25
	756	781	1.03	854	5	30	5.04	1.03	0.79	25
	849	854	1.01	854	5	30	3.08	1.42	0.85	25
	838	854	1.02	854	5	30	3.71	1.42	0.81	25
	829	854	1.03	854	5	30	3.80	1.42	0.84	25
	815	854	1.05	854	5	30	3.96	1.42	0.84	25
	750	810	1.08	854	5	30	6.30	1.42	0.75	25
Heat input investigation	827	854	1.03	854	5	100	3.46	1.12	0.83	25
	808	849	1.05	854	5	50	3.46	1.12	0.83	25
	823	836	1.02	854	5	30	3.46	1.12	0.83	25
	812	814	1.00	854	5	12	3.46	1.12	0.83	25
	807	798	0.99	854	5	6	3.46	1.12	0.83	25
	804	850	1.06	854	5	100	4.15	1.12	0.82	25
	797	833	1.04	854	5	50	4.15	1.12	0.82	25
	795	820	1.03	854	5	30	4.15	1.12	0.82	25
	799	799	1.00	854	5	12	4.15	1.12	0.82	25

	787	783	1.00	854	5	6	4.15	1.12	0.82	25
	801	834	1.04	854	5	100	4.45	1.12	0.80	25
	800	817	1.02	854	5	50	4.45	1.12	0.80	25
	792	805	1.02	854	5	30	4.45	1.12	0.80	25
	785	784	1.00	854	5	12	4.45	1.12	0.80	25
	769	769	1.00	854	5	6	4.45	1.12	0.80	25
	797	821	1.03	854	5	100	4.74	1.12	0.78	25
	778	805	1.03	854	5	50	4.74	1.12	0.78	25
	776	793	1.02	854	5	30	4.74	1.12	0.78	25
	763	773	1.01	854	5	12	4.74	1.12	0.78	25
	754	758	1.00	854	5	6	4.74	1.12	0.78	25
Bevel shape and matching type investigation (V- and X-groove)	876	844	0.96	883	10	10	2.62	1.09	0.80	25
	829	801	0.97	883	10	10	3.85	1.09	0.76	25
	809	776	0.96	883	10	10	4.95	1.09	0.74	25
	778	761	0.98	883	10	10	5.23	1.09	0.71	25
	863	813	0.94	883	10	10	3.59	1.09	0.78	25
	831	821	0.99	883	10	10	2.87	1.09	0.77	25
	808	793	0.98	883	10	10	4.11	1.09	0.75	25
	793	785	0.99	883	10	10	4.83	1.09	0.75	25
	783	799	1.02	883	10	10	3.56	1.09	0.75	25
	875	883	1.01	883	10	10	2.25	1.37	0.81	25
	858	841	0.98	883	10	10	3.59	1.37	0.74	25
	832	828	1.00	883	10	10	4.21	1.37	0.73	25
	791	825	1.04	883	10	10	5.01	1.37	0.74	25
	881	883	1.00	883	10	10	2.35	1.37	0.86	25
	863	883	1.02	883	10	10	3.50	1.37	0.84	25
	850	880	1.04	883	10	10	3.69	1.37	0.82	25
	828	865	1.04	883	10	10	4.05	1.37	0.80	25
	805	883	1.10	883	10	10	3.55	1.37	0.83	25
Chen et al. [24]										
BJ8-4	687	681	0.99	838	8	12.5	7.69	1.01	0.69	30
BJ12-5	698	687	0.98	838	12	12.5	7.03	1.01	0.68	30
BJ16-3.2	773	720	0.93	838	16	12.5	5.04	1.01	0.71	30
BJ16-4	745	732	0.98	838	16	12.5	4.63	1.01	0.72	30
BJ16-5	721	741	1.03	838	16	12.5	4.88	1.01	0.74	30

Note: “Exp” is the experimental ultimate strength of the butt-welded specimen;
“Pre” is the predicted ultimate strength of the butt-welded specimen ; .
“BA” is the bevel angle of the weld.

References

[1] R. Stroetmann, T. Kästner, A. Hälsig, P. Mayr, Influence of the cooling time on the mechanical properties of welded HSS-joints, Steel Constr. 11 (2018) 264–271, https://doi.org/10.1002/stco.201800019.

[2] W. Cai, Y. Wang, G. Li, R. Stroetmann, Comparative study on strength of TMCP and QT high-strength steel butt-welded joints, J. Constr. Steel Res. 197 (2022), 107447, https://doi.org/10.1016/j.jcsr.2022.107447.

[3] M. Amraei, A. Ahola, S. Afkhami, T. Björk, A. Heidarpour, X.L. Zhao, Effects of heat input on the mechanical properties of butt-welded high and ultra-high strength steels, Eng. Struct. 198 (2019), https://doi.org/10.1016/j.engstruct.2019.109460.

[4] H.C. Ho, K.F. Chung, M.X. Huang, D.A. Nethercot, X. Liu, H. Jin, G.D. Wang, Z. H. Tian, Mechanical properties of high strength S690 steel welded sections through tensile tests on heat-treated coupons, J. Constr. Steel Res. 166 (2020), 105922, https://doi.org/10.1016/j.jcsr.2019.105922.

[5] X. Liu, K.F. Chung, H.C. Ho, M. Xiao, Z.X. Hou, D.A. Nethercot, Mechanical behavior of high strength S690-QT steel welded sections with various heat input energy, Eng. Struct. 175 (2018) 245–256, https://doi.org/10.1016/j.engstruct.2018.08.026.

[6] R. Yan, H. Xin, F. Yang, H. El Bamby, M. Veljkovic, K. Mela, A method for determining the constitutive model of the heat-affected zone using digital image correlation, Constr. Build. Mater. 342 (2022), 127981, https://doi.org/10.1016/j.conbuildmat.2022.127981.

[7] V.P. Nguyen, Effect of heat input on the mechanical properties of welded joints. https://urn.fi/URN:NBN:fi:amk-2018091915234, 2018.

[8] Y.H. Cho, L.H. Teh, B. Young, A. Ahmed, Net section tension strength of bolted connections in ultra-high strength sheet steel during and after fire, J. Constr. Steel Res. 172 (2020), https://doi.org/10.1016/j.jcsr.2020.106237.

[9] X. Xue, Y. Shi, X. Zhou, J. Wang, Y. Xu, Experimental study on the properties of Q960 ultra–high–strength steel after fire exposure, Structures. 47 (2023) 2081–2098, https://doi.org/10.1016/j.istruc.2022.12.034.

[10] R. Yan, H. El Bamby, M. Veljkovic, H. Xin, F. Yang, A method for identifying the boundary of regions in welded coupon specimens using digital image correlation, Mater. Des. 210 (2021), 110073, https://doi.org/10.1016/j.matdes.2021.110073.

[11] R. Yan, K. Mela, F. Yang, H. El Bamby, M. Veljkovic, Equivalent material properties of the heat-affected zone in welded cold-formed rectangular hollow section connections, Thin-Walled Struct. 184 (2023), 110479, https://doi.org/10.1016/j.tws.2022.110479.

[12] R. Yan, H. El Bamby, M. Veljkovic, Experimental and numerical study of butt welded joints made of high strength steel, in: The Eighth International Conference on Structural Engineering, Mechanics and Computation, 2022, https://doi.org/10.1201/9781003348443-190.

[13] F. Hochhauser, W. Ernst, R. Rauch, R. Vallant, Influence of the soft zone on the strength of welded modern HSLA steels, Weld. World. 56 (2012), https://doi.org/10.1007/BF03321352.

[14] X. Zhao, Study on Mechanical Properties and Design Method of over 500MPa High Strength Steel Butt Welded Connections, Tongji University, 2020.

[15] W.Y. Cai, Y.B. Wang, G.Q. Li, Experimental and numerical study on strength of high-strength steel double-V butt-welded joint, J. Constr. Steel Res. 196 (2022), 107397, https://doi.org/10.1016/j.jcsr.2022.107397.
[16] L. Zhang, T. Kannengiesser, HAZ softening in Nb-, Ti- and Ti + V-bearing quenched and tempered steel welds, Weld. World. 60 (2016) 177–184, https://doi.org/10.1007/s40194-016-0299-7.
[17] M. Khurshid, Z. Barsoum, I. Barsoum, Load Carrying Capacities of Butt Welded Joints in High Strength Steels 137, 2015, pp. 1–9, https://doi.org/10.1115/1.4030687.
[18] L. Keränen, O. Nousiainen, V. Javaheri, A. Kaijalainen, A.P. Pokka, M. Keskitalo, J. Niskanen, E. Kurvinen, Mechanical properties of welded ultrahigh-strength S960 steel at low and elevated temperatures, J. Constr. Steel Res. 198 (2022), 107517, https://doi.org/10.1016/j.jcsr.2022.107517.
[19] C. Chen, S.P. Chiew, M.S. Zhao, C.K. Lee, T.C. Fung, Welding effect on tensile strength of grade S690Q steel butt joint, J. Constr. Steel Res. 153 (2019) 153–168, https://doi.org/10.1016/j.jcsr.2018.10.009.
[20] P. Collin, M. Möller, M. Nilsson, S. Törnblom, Undermatching Butt Welds in high strength steel, IABSE Symposium, Bangkok 2009: Sustainable Infrastructure - Environment Friendly, Safe Resourc. Effic. 96 (2009) 96–106, https://doi.org/10.2749/222137809796078829.
[21] F. Sun, M. Ran, G. Li, R.Y. Xiao, Y. Wang, Experimental and numerical study of high-strength steel butt weld with softened HAZ, Proc. Inst. Civ. En.: Struct. Build. 171 (2018) 583–597, https://doi.org/10.1680/jstbu.16.00102.
[22] M.M. Ran, F.F. Sun, G.Q. Li, A. Kanvinde, Y.B. Wang, R.Y. Xiao, Experimental study on the behavior of mismatched butt welded joints of high strength steel, J. Constr. Steel Res. 153 (2019) 196–208, https://doi.org/10.1016/j.jcsr.2018.10.003.
[23] W.M. Maurer, Untersuchung der Auswirkung einer Weichen Zone auf die Festigkeitseigenschaften von hochfesten Schweißverbindungen Kurzfassung, 2014.
[24] C. Chen, S.P. Chiew, M.S. Zhao, C.K. Lee, T.C. Fung, Influence of cooling rate on tensile behaviour of S690Q high strength steel butt joint, J. Constr. Steel Res. 173 (2020), 106258, https://doi.org/10.1016/j.jcsr.2020.106258.
[25] A. Khalfallah, Experimental and numerical assessment of mechanical properties of welded tubes for hydroforming, Mater. Des. 56 (2014) 782–790, https://doi.org/10.1016/j.matdes.2013.11.051.
[26] M.L. Zhu, F.Z. Xuan, Correlation between microstructure, hardness and strength in HAZ of dissimilar welds of rotor steels, Mater. Sci. Eng. A 527 (2010) 4035–4042, https://doi.org/10.1016/j.msea.2010.03.066.
[27] Y. Peng, C. Wu, J. Gan, J. Dong, Characterization of heterogeneous constitutive relationship of the welded joint based on the stress-hardness relationship using micro-hardness tests, Constr. Build. Mater. 202 (2019) 37–45, https://doi.org/10.1016/j.conbuildmat.2018.12.218.
[28] prEN 1993-1-8:2021 - Design of steel structures - Part 1–8: Design of joints (draft of EN1993-1-8: 2021), 2022.
[29] ABAQUS, ABAQUS Analysis User's Manual, 2021 Version, 2021.
[30] prEN 1993-1-1 Eurocode 3 — Design of steel structures — Part 1–1: General rules and rules for buildings, 2021.
[31] H.W. Swift, Plastic instability under plane stress, J. Mech. Phys. Solids. 1 (1952) 1–18, https://doi.org/10.1016/0022-5096(52)90002-1.
[32] A. Considère, Annales des Ponts et Chaussées 9, 1885, pp. 574–775.
[33] R. Yan, H. Xin, K. Mela, H. El Bamby, M. Veljkovic, Fracture simulation of welded RHS X-joints using GTN damage model, Adv. Struct. Eng. 0 (2022) 1–20, https://doi.org/10.1177/13694332221137175.
[34] E. Voce, The relationship between stress and strain for homogeneous deformation, J. Inst. Met. 74 (1948) 537–562.
[35] E.J. Pavlina, C.J. Van Tyne, Correlation of yield strength and tensile strength with hardness for steels, J. Mater. Eng. Perform. 17 (2008) 888–893, https://doi.org/10.1007/s11665-008-9225-5.
[36] D. Tabor, The Hardness of Metals, Oxford University Press, 1951.